Applied Surface Science 331 (2015) 285–291

Contents lists available at ScienceDirect

Applied Surface Science

journal homepage: www.elsevier.com/locate/apsusc

Alloyed nanoparticle-embedded alumina nanocermet film: A new attempt to improve the thermotolerance

C.J. Tu[a,b], J.H. Gao[b], S. Hui[a,b], D. Lou[a], H.L. Zhang[b], L.Y. Liang[b], A.P. Jin[c], Y.S. Zou[a,*], H.T. Cao[b,*]

[a] School of Materials Science and Engineering, Institute of Optoelectronics and Nanomaterials, Nanjing University of Science and Technology, Nanjing, Jiangsu 210094, China
[b] Division of Functional Materials and Nano Devices, Ningbo Institute of Material Technology and Engineering, Chinese Academy of Sciences, Ningbo 315201, China
[c] School of Chemistry and Chemical Engineering, Wuhan Textile University, Wuhan, Hubei 40073, China

ARTICLE INFO

Article history:
Received 30 September 2014
Received in revised form
25 December 2014
Accepted 10 January 2015
Available online 17 January 2015

Keywords:
Silver nanoparticles
Nanocermet
Resonance absorption
Bimetallic alloy
Thermal stability

ABSTRACT

This paper focuses on the enhancement of thermal stability of Ag-Al_2O_3 nanocermet films by means of alloying of Ag nanoparticles with Al element. The optical analysis demonstrated the AgAl embedded Al_2O_3 cermet films (namely, AgAl-Al_2O_3) possess excellent thermal tolerance even at 500 °C for 260 h under nitrogen ambient. The evolution of microstructural and chemical properties of Al_2O_3/AgAl-Al_2O_3/Al_2O_3 stack layers during the annealing process was comprehensively investigated, in order to grasp the thermal stability mechanism. It is believed that the enhanced thermal stability was ascribed to the formation of fresh alumina as capping layer riveted on the Ag nanoparticles surfaces, which acted as the pinning points to prevent silver element from migrating so as to maintain the expected optical properties.

1. Introduction

Silver nanoparticles have attracted considerable interests because of absorption resonance (also donated as plasmon resonance) phenomenon [1–3]. This resonance is attributed to the inherent oscillation of free-like electrons on nanoparticle or cluster surfaces excited by the electromagnetic light wave, resulting in wavelength-selective photon absorption and resonant Mie scattering [4]. Due to the unique optical properties, silver nanoparticles embedded in a ceramic matrix (e.g. Al_2O_3 or SiO_2) are utilized to construct nanocermet absorbing layers for solar thermal applications. In general, the optical properties of the nanocermets are closely related to the shape, size and size distribution of the metallic particles, and the interaction between the dielectric matrix and metallic spheres as well [5,6]. In the last decade, various Ag-based nanocermet system including Ag-Al_2O_3 [7], Ag-TiO_2 [8], Ag-Si_3N_4 [9], Ag-SiO_2 [10], Ag-Bi_2O_3 [11] *etc.* has been developed, showing desirable light absorption and great potential for solar energy conversion.

The microstructual and chemical compositional stability of Ag-based nanocermet must be closely concerned, so as to maintain its performance at high temperatures. Unfortunately, however, as a metal with low melting temperature (about 960 °C), Ag nanoparticles are easily subjected to agglomeration and outwards diffusion when working at elevated temperatures, which would limit their high-temperature applications [12–16]. Barshilia et al. [7] have clearly pointed out that Ag-Al_2O_3 coatings have dramatic degradation at higher temperatures (>400 °C) due to the defragmentation of the Ag nanoparticles in the dielectric matrix. For the Ag-Al_2O_3 nanocermet, the key issue is to ensure their high temperature thermal stability. Since Al_2O_3 exhibits excellent stability at high temperatures, the thermal stability of the nanocermet mainly depends on the thermal tolerance of Ag nanoparticles. Xiao et al. [12] believed that the agglomeration of Ag nanoparticles was favorable to improving the thermal resistance of Ag-Al_2O_3 nanocermets due to the low surface free energy of the agglomerates. However, simply increasing the size of the Ag nanoparticles would become invalid eventually after long-term annealing, so it is not an appropriate solution.

* Corresponding authors. Tel.: +86 25 84313349; fax: +86 25 84303279.
E-mail addresses: yshzou75@gmail.com (Y.S. Zou), h.cao@nimte.ac.cn (H.T. Cao).

http://dx.doi.org/10.1016/j.apsusc.2015.01.064
0169-4332/

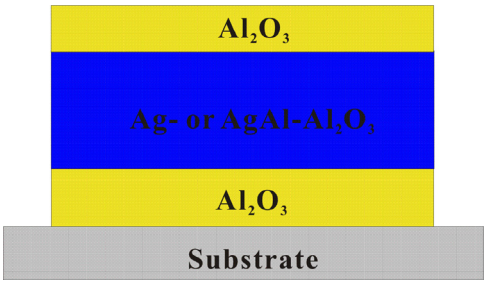

Fig. 1. Schematic diagram of the sandwich structure for thermal stability investigations.

Alloying is an effective solution to improve the thermal stability of Ag nanoparticles [13–15]. It was suggested that AgAl alloy films showed high thermal tolerance even at 600 °C [15–17]. The reasons are either the appearance of stable alloy phase of Ag_2Al during annealing or the oxidation of Al to passivate grain-boundaries and surfaces of the film [16,17]. In our previous work [18], we attempted to use AgAl bimetallic alloy nanoparticles to fabricate AgAl-Al_2O_3 nanocermet, featuring good thermal tolerance annealed at 500 °C for 130 h. Furthermore, the constructed solar absorbers based on AgAl-Al_2O_3 absorbing layers exhibited high absorptance (α = 94.2%) and low thermal emittance (ε = 15%) after annealed at 450 °C for 70 h in N_2. However, both the time evolution processes of bimetallic alloy nanoparticles and the thermal stability mechanism haven't been clarified yet. In this paper, we presented a detailed study on the evolution of the optical properties, microstructure and chemical composition of the AgAl-Al_2O_3 films during the annealing processes. The thermal stability mechanism was also discussed.

2. Experimental details and characterization

Ag- or AgAl-Al_2O_3 thin films were deposited onto (1 0 0) silicon, porous carbon grids or quartz by a magnetron sputtering system (Jsputter8000, manufactured by ULVACCo., Ltd.) at room temperature. Highly pure Ag (purity = 99.99%), Al (purity = 99.99%) and Al_2O_3 targets (purity = 99.99%) were used as the sputtering sources. The Ag and Al_2O_3 targets were operated by two RF power supplies while a DC power was used to sputter the Al target. The substrates were ultrasonically cleaned by using alcohol and acetone in an ultrasonic agitator before loading them into the vacuum chamber. Prior to the deposition process, the chamber was pumped down to a base pressure of 2×10^{-4} Pa.

To eliminate the influence of the environment and substrates, a sandwich structure was utilized, which is consisted of a bottom layer (Al_2O_3, around 17 nm), a middle selective absorbing layer (Ag- or AgAl-Al_2O_3, around 50 nm), and a top layer (Al_2O_3, around 11 nm), as seen in Fig. 1. The films were deposited at a pressure of 0.22 Pa in Ar plasma. The detail processing conditions are listed in Table 1. In order to make the films homogeneous and uniform, the substrate was rotated at a speed of 20 rpm. In addition, for investigating the influence of the additive Al on the surface morphology, single Ag-Al_2O_3 and AgAl-Al_2O_3 absorbing layers were directly deposited on silicon for 55 min or porous carbon grids for 5 min, respectively.

To characterize the thermal stability, the Ag-Al_2O_3 and AgAl-Al_2O_3 samples with a sandwich structure were first pretreated in turn at 200 and 300 °C in air for 2 h, then they were annealed at 500 °C in a nitrogen atmosphere with different durations.

The topography of the Ag-Al_2O_3 or AgAl-Al_2O_3 single layer was performed using atomic force microscopy (AFM, Dimesion-3100 Scanning Probe Microscope) operating in a tapping mode with the scan size of 5 μm × 5 μm. The diameters of the nanoparticles showed in the AFM images were estimated by the height value. To observe the nanoscale particles, transmission electron microscopy (TEM) images were recorded using TF20 instrument at an accelerating voltage of 200 kV on the porous carbon grids. The optical absorption spectra of the sandwich samples were measured with a Lambda 950 UV–vis-NIR spectrophotometer in the wavelength range of 300–2500 nm. Furthermore, Scanning electron microscopy (SEM) analysis was carried on a SEM-S4800 instrument operating at 5 kV to characterize the surface micrographs of the sandwich structure. The phase structure of thin films was examined using a D8 Discover type X-ray diffraction (XRD) at a glancing angle of 0.5° with Cu K_α radiation (λ = 0.15406). X-ray photoelectron spectroscopy (XPS, AXIS UTLTRA DLD) analysis was carried out by use of Al K_α X-ray (1486.6 eV) to determine the chemical compositions of the sandwiched films.

3. Results and discussion

3.1. Optical properties

Fig. 2 displays the evolution of the absorption spectra of the Ag-Al_2O_3 and AgAl-Al_2O_3 thin films on quartz under different annealing conditions. The sandwich structure was shown in Fig. 1. The absorption $A(\lambda)$ of the samples was calculated following $A(\lambda) = 1 - (R(\lambda) + T(\lambda))$ from the measured reflectance $R(\lambda)$ and transmittance $T(\lambda)$ spectra at the wavelength λ ranging from 300 to 2500 nm. Measurements of the reflectivity and transmitivity were done at an angle of 8° and 0° with respect to the normal, respectively. It can be observed that there is a broad absorption peak located at 387 nm for the as-deposited Ag-Al_2O_3 thin films, which

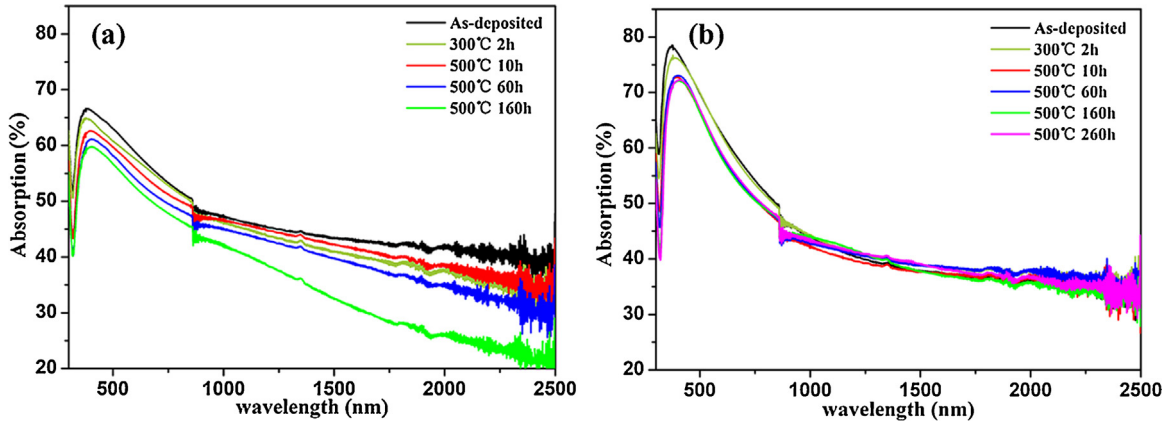

Fig. 2. The absorption spectra of Ag-Al_2O_3 (a) and AgAl-Al_2O_3 (b) samples during annealing.

Table 1
The detail deposition parameters for Ag-Al_2O_3 and AgAl-Al_2O_3 samples.

Layers	Al_2O_3 target (W)	Ag target (W)	Al target (W)	Sputtering time (min)	RF bias (W)
Al_2O_3 top layer	115	0	0	20	10
Ag- or AgAl-Al_2O_3 absorbing layer	115	9	0 or 8	55	0
Al_2O_3 bottom layer	115	0	0	30	10

is due to the resonance absorption of Ag nanoparticles. In comparison, however, the absorption peak of as-fabricated AgAl-Al_2O_3 thin films exhibits a slight blue shift from 387 nm to 378 nm and the absorbance increases from 66.5% to 78.3%.

After pretreated in turn at 200 and 300 °C in air for 2 h, the absorption peak position of the Ag-Al_2O_3 sample shifts from 387 nm to 376 nm. Simultaneously, the absorbance reduces from 66.5% to 64.8% (Fig. 2a), in accordance with the previous report [19,20]. However, for the AgAl-Al_2O_3 case, a red-shift of the absorption peak from 378 to 386 nm together with an absorbance decreasing from 78.3% to 76.2% can be observed, as shown in Fig. 2b. Then the absorption peaks of the both samples display a red-shift to 400 nm and a decrease in absorbance after annealing at 500 °C in N_2 for 10 h. This red-shift of silver absorption peak has also been observed by Yeshchenko et al. [21]. With further extending the annealing time (@500 °C), a sharp decrease in absorbance, especially at $\lambda > 450$ nm, as well as a slight peak position blue-shift are observed for the Ag-Al_2O_3 specimen. The resonance absorption peak position of Ag-Al_2O_3 thin films shifted substantially during the annealing processes, indicating that Ag nanoparticles in the alumina matrix were fairly unstable. However, for the AgAl-Al_2O_3 sample, the absorbance and the peak position keep almost constant even after prolonging the annealing time to 260 h, suggesting that AgAl-Al_2O_3 thin film possesses excellent thermal stability at 500 °C.

3.2. Microstructure and chemical composition

Generally, the thermal tolerance capacity of the nanoparticles is closely coupled with their morphological evolution [22]. Fig. 3a–d illustrates the AFM surface morphologies of the as-deposited Ag-Al_2O_3 and AgAl-Al_2O_3 thin films and their corresponding particle-size distribution histograms. Both the samples were directly deposited on Si substrate with a single layer structure. The nanoscale particles in the as-deposited samples, prepared on porous carbon grids for 5 min, were further observed by TEM (see Fig. 3e and f), indicating that lots of silver nanoparticles are small with a diameter below 20 nm. It can be found that Ag nanoparticles are randomly dispersed in the ceramic matrix with a wide range of particle size distribution. Compared to the Ag-Al_2O_3 thin film shown in Fig. 3a, the statistical population of metal nanoparticles in the AgAl-Al_2O_3 thin film (Fig. 3b, e and f) increased, indicating that the addition of Al can allow the easier nucleation and growth of nanoparticles. On one hand, Ag and Al possess the similar Face-Center Cubic (FCC) structure with almost the same lattice constant (0.408 [23] and 0.405 [24], respectively); on the other, Al element is easily dissolved in Ag [25], so it is reasonably believed that the AgAl alloyed nanoparticles are easily formed and the nucleation of the AgAl nanoparticles features a heterogeneous nucleation mode. Furthermore, the average size of the AgAl nanoparticles decreases to some extent, ranging from 46 to 33 nm (Fig. 3c and d). According to the-above observations, one can conclude that the alloyed AgAl nanoparticles with relatively smaller diameter have a higher dispersed density within the host matrix.

SEM images are exhibited in order to make the morphology evolution clearer. The samples are also with a sandwich structure (as shown in Fig. 1), which were firstly pretreated in turn at 200 and 300 °C in air for 2 h and then annealed at 500 °C in N_2 for 10 h. The inset graphs show the high-resolution images of the corresponding samples. Fig. 4a–c shows the SEM images of the as-deposited and annealed Ag-Al_2O_3 samples. The size distribution of Ag nanoparticles is given in Fig. 5a–c. When Ag-Al_2O_3 specimen was pretreated in turn at 200 and 300 °C in air for 2 h, relatively small changes in the morphology features can be observed as compared to the as-deposited one. In particular, the average particle size of the former case is about 174 nm (Fig. 5b). After annealing at 500 °C in N_2 for 10 h, however, the average particle size is sharply increased to be about 970 nm (Fig. 5c). These results confirmed that Ag particles are easily subjected to diffusion and agglomeration via Ostwald ripening process during the annealing process, resulting in considerable particle size growth as expected. The prominent change in their microstructure was the agglomeration of nanoparticles, in order to decrease the system free energy [26]. This continuous size increasing led to the absorption peak blue-shift firstly and red-shift afterward, as presented in Fig. 2a. The blue-shift happened in the pretreatment process was ascribed to the intrinsic size effect [27]. As the particle size exceeded a certain threshold (>50 nm), however, the external size effect would result in the red-shift of the peak position (seen in Fig. 2a) [28,29].

Fig. 4d-f and Fig. 5d-f show the SEM images and the corresponding size distribution of nanoparticles in the AgAl-Al_2O_3 samples before and after annealing, respectively. The average particle size of the as-deposited and pretreated sample is 49.6 nm and 103 nm (see Fig. 5d and e), respectively. After annealing at the 500 °C for 10 h, the surface morphology does not change apparently as compared with the pretreated one. For example, the average particle size after 500 °C annealing slightly increases to be 137 nm (Fig. 5f). The above SEM images confirm that the thermal agglomeration was dramatically alleviated in the AgAl-Al_2O_3 samples.

A detailed evolution of the phase structure in the nanocermet samples was characterized by XRD measurements. Fig. 6 shows the XRD pattern profiles of the Ag-Al_2O_3 and AgAl-Al_2O_3 samples, which are the same as shown in Fig. 2. The diffraction peaks corresponding to (1 1 1), (2 2 0) and (2 0 0) Ag planes (the PDF #65-2871) can be observed, showing a typical FCC-type structure. It can be seen that the diffraction peaks of both the as-deposited samples are very broad with low intensity, indicating that the metallic nanoparticles are finely dispersed in the amorphous Al_2O_3 matrix [30]. The particle size is calculated to be about 2.5–4 nm by using the Debye–Scherer approximation, consistent with the results obtained from TEM (see Fig. 3e and f). After the samples are pretreated in turn at 200 and 300 °C in air for 2 h, both the samples show inconspicuous changes, e.g., the particle size is increased slightly to be about 3.5–5 nm in diameter. For the Ag-Al_2O_3 sample after annealing at 500 °C in N_2 ambient for 2 h (Fig. 6a), the intensity of (1 1 1) diffraction peak increases apparently as a result of the grain growth (grain size about 60 nm). However, the intensity of the peak at 38.1° begins to decrease monotonically with extending the annealing time. Only one weak peak of (1 1 1) plane can be observed after annealing at 500 °C for 62 h. The time evolution of diffraction peak suggests that the volume fraction of Ag is gradually reduced, which in turn is stemmed from the outwards diffusion and even evaporation of the Ag elements [12,31,32]. The loss of Ag would aggravate the optical degradation of the Ag-Al_2O_3 films during the long-time annealing, as shown in Fig. 2a. For the AgAl-Al_2O_3 sample (Fig. 6b), the XRD patterns become sharper after annealing at 500 °C for 2 h. With prolonging the duration, the intensity of the

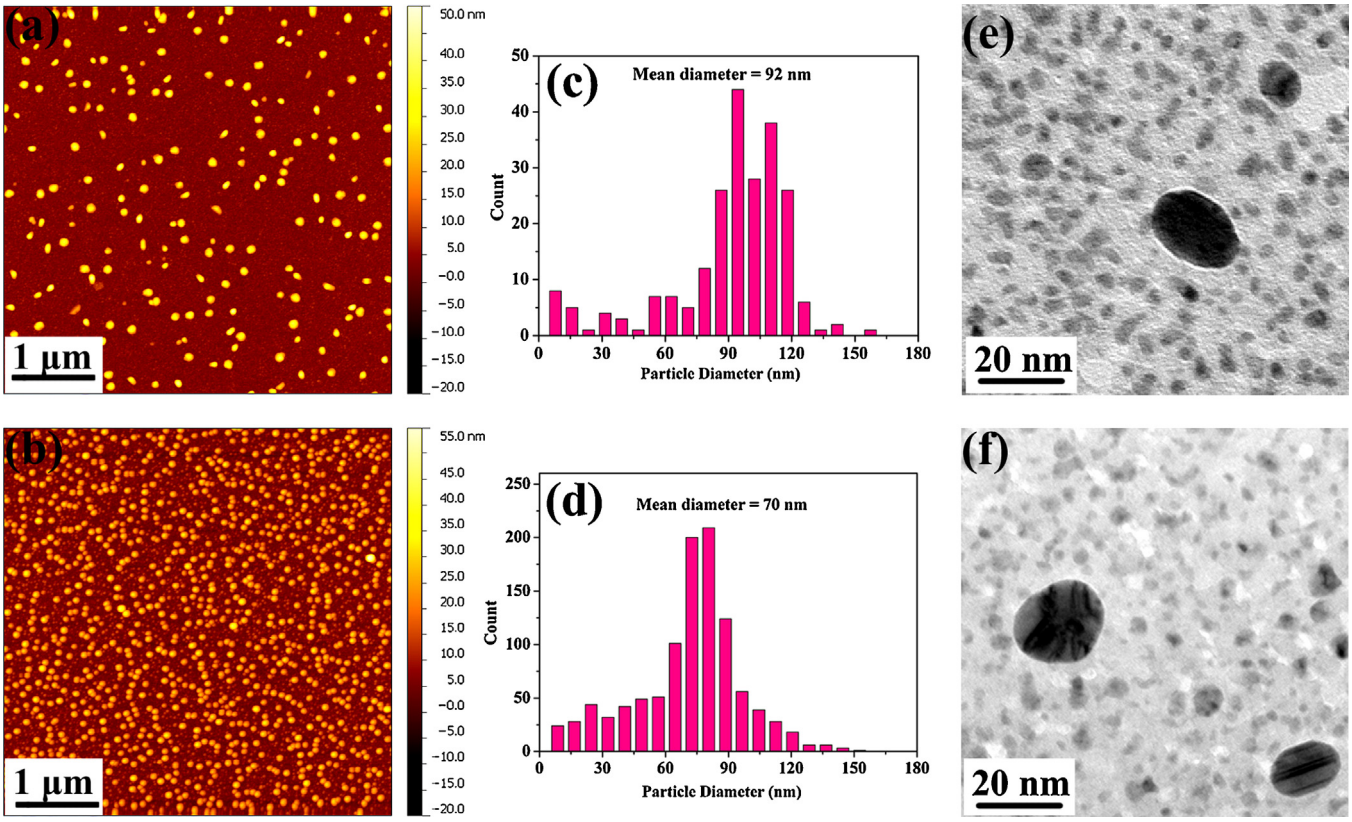

Fig. 3. AFM topographic images of single-layer Ag-Al_2O_3 (a) and AgAl-Al_2O_3 (b) thin films deposited on Si substrate, and the corresponding histograms of the nanoparticles (c) (d) and TEM images (e) (f).

diffraction peaks tends to be constant even after annealing for 160 h. The peaks of (1 1 1), (2 0 0) and (2 2 0) planes are all clear to see. It should be pointed out that there is no detectable diffraction peak of Al_2O_3, meaning that the Al_2O_3 is amorphous during the annealing process. The phase structure stability confirms again that the thermal stability of Ag nanoparticles is strengthened by addition of Al, in line with the absorption spectra.

Fig. 7 shows the element distribution profile of Ag, Al and O in the AgAl-Al_2O_3 sample before and after annealing at 500 °C in N_2. The annealed sample was pretreated in turn at 200 and 300 °C in air for 2 h. After data acquisition at the topmost surface, the XPS measurements were recorded after each step with Ar plasma etching for 45 s. Compared with the as-deposited case, the distribution profile of Ag in the annealed sample does not show any obvious changes, although a certain amount of Ag distribution is detected

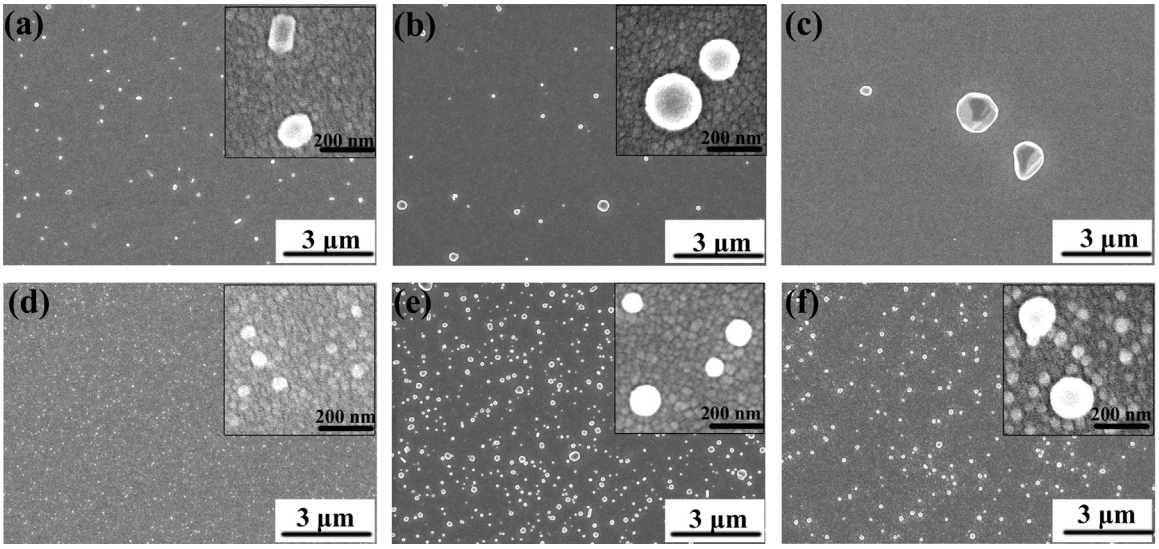

Fig. 4. SEM images of as-deposited and annealed samples at different annealing conditions: (a) Ag-Al_2O_3, as-deposited; (b) Ag-Al_2O_3, 300 °C in air for 2 h; (c) Ag-Al_2O_3, 500 °C in N_2 for 10 h; (d) AgAl-Al_2O_3, as-deposited; (e) AgAl-Al_2O_3, 300 °C in air for 2 h; (f) AgAl-Al_2O_3, 500 °C in N_2 for 10 h. The inset graphs show the high-resolution images of the corresponding samples.

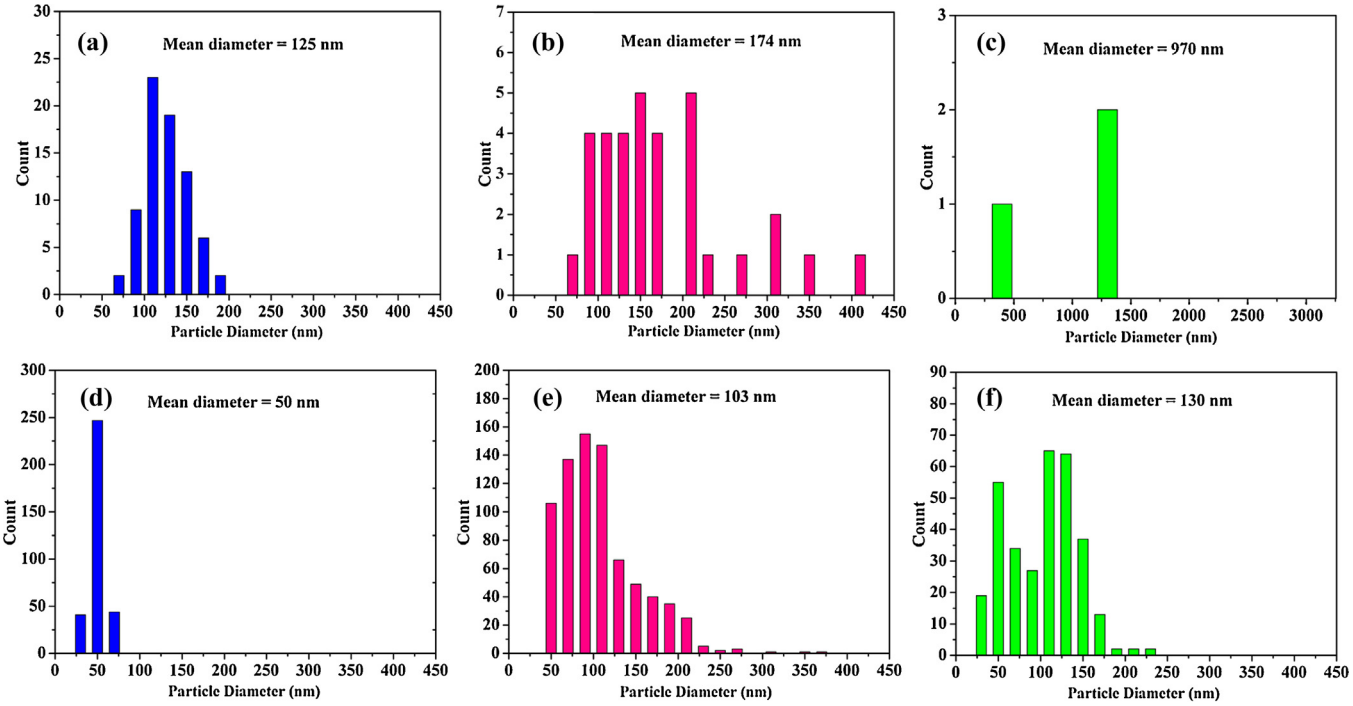

Fig. 5. The average size distribution of Ag nanoparticles: (a) Ag-Al_2O_3, as-deposited; (b) Ag-Al_2O_3, 300 °C in air for 2 h; (c) Ag-Al_2O_3, 500 °C in N_2 for 10 h; (d) AgAl-Al_2O_3, as-deposited; (e) AgAl-Al_2O_3, 300 °C in air for 2 h; (f) AgAl-Al_2O_3, 500 °C in N_2 for 10 h.

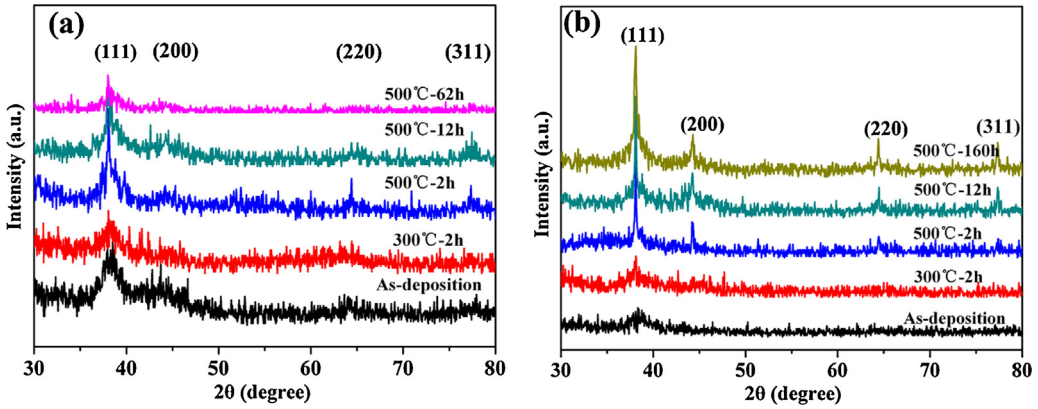

Fig. 6. The evolution of XRD diffraction patterns of Ag-Al_2O_3 (a) and AgAl-Al_2O_3 (b) samples during annealing.

on the top face of the sandwich structure. This phenomenon has also been observed by Xiao et al. [12].

Further investigation on the chemical state of Al was performed to explore the effect of the Al additive on improving the thermal stability of the AgAl-Al_2O_3 nanocermet. Fig. 8 displays the binding energies for the Al 2*p* core level peaks of the AgAl-Al_2O_3 samples before and after annealing, corresponding to the Fig. 7a and b, respectively. The XPS measurement was recorded after each

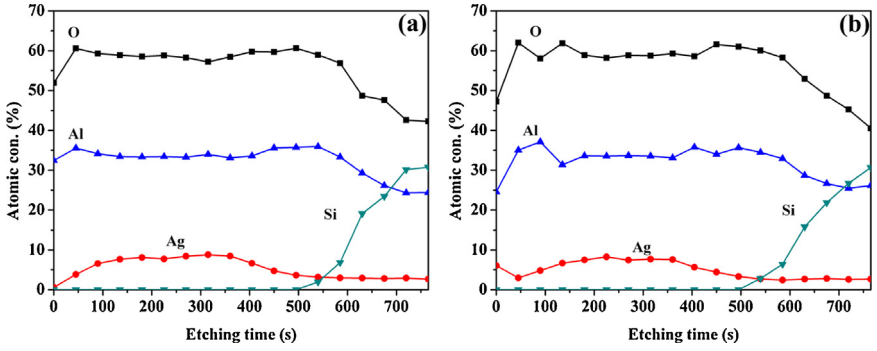

Fig. 7. The distribution profile of Ag, Al and O element in the AgAl-Al_2O_3 sample before (a) and after annealing at 500 °C in N_2 (b).

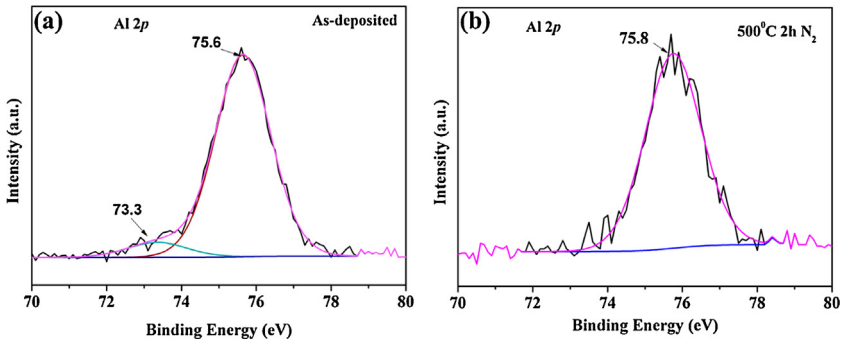

Fig. 8. The binding energies for the Al 2*p* core level peaks of the AgAl-Al_2O_3 film before (a) and after annealing at 500 °C in N_2 (b).

etching step (315 s). In the as-deposited sample (see Fig. 8a), two Al 2*p* core level peaks centered at 73.3 eV and 75.6 eV were observed. It is known that the binding energies of Al 2*p* core level peak are in a range of 72.4–73.1 eV for the metallic Al and in a range of 75.9–76.6 eV for the oxidized state [33], respectively. Thus, the Al 2*p* peak at 73.3 eV and 75.6 eV is presumably from metallic Al and oxidized Al, respectively, indicating that the metallic Al is present in the as-deposited AgAl-Al_2O_3 specimen. The metallic Al/Ag atomic ratio was calculated to be about 18%. But nevertheless, only Al 2p core level peak for alumina is observed in the annealed sample (shown in Fig. 8b), implying that the metallic Al is oxidized during the annealing process. This behavior is consistent with the previous study on oxidation-driven restructuring of Au-Cu bimetallic nanoparticles embedded in SiO_2 [34].

Based upon the above discussion, thermal induced diffusion of Ag element during annealing was the main reason to account for the optical property degradation. Thus, the improved thermal stability of AgAl-Al_2O_3 thin film was associated with the effective delay on Ag diffusion. It was confirmed by the XPS analysis that the oxidation of the metallic Al played an important role in inhibiting Ag migration. Firstly, Al was dissolved in Ag particles to form AgAl alloy nanoparticles. Secondly, the solute Al in the alloy nanoparticles diffused outward preferentially and then got oxidized near the particle surface during pretreatment in air, which is analogous to the restructuring behavior of other alloy nanoparticles driven by oxidation [34,35]. The freshly generated alumina, regarded as the armor layer covering the alloy nanoparticles, raised the diffusion barrier to inhibit the migration of the Ag element so as to sustain the optical signals [18]. It should be pointed out that the alloying process was not fully completed, in other words, there were some unalloyed pure Ag particles within the host matrix, which was evidenced by the obvious growth of small particles in the insert to Fig. 4e and f. From a global perspective, the present of Ag agglomerates in the AgAl-Al_2O_3 nanocermet cannot be ruled out, but these agglomerates were isolated among the armor layer-capped particles, so the microstructure changes were reduced as marginally as possible, which leads to the superior thermal stability.

4. Conclusion

In this work, we comprehensively investigated the thermal stability of Ag or AgAl nanoparticle embedded alumina matrix. The AgAl-Al_2O_3 films exhibited appreciable thermal stability even after annealing at 500 °C for 260 h. The detailed studies of surface micrograph and crystalline structure of the AgAl-Al_2O_3 film throughout the whole annealing processes were performed, in order to find out the thermal stability origin. The diffusion, agglomeration and evaporation of the Ag nanoparticles observed in Ag-Al_2O_3 films during annealing, were significantly suppressed in the AgAl-Al_2O_3 case. It was proposed that the metallic Al diffused out of AgAl alloy nanoparticles after the low-temperature pretreatment in air, and got oxidized on the interfacial sites between the particles and the alumina matrix. The freshly generated alumina, acting as an armor layer on the alloy nanoparticles, was pinned against the matrix and could prevent Ag element from long-distance diffusion. These investigations are beneficial for deeply understanding the effects of the Al additive on improving the thermal stability of Ag-Al_2O_3 films, which would offer a brand new idea for designing high-temperature-endurable nanocermet materials for solar thermal applications.

Acknowledgments

We acknowledge the financial support from the National Natural Science Foundation of China (Grant No. 51302277 and 51102187), the Applied Research Funds for Public Welfare Project of Zhejiang Province (Grant No. 2014C31148), the Ningbo Natural Science Foundation (Grant No. 2013A610073) and the Project funded by China Postdoctoral Science Foundation (Grant No. 2013M541808).

References

[1] M. Jasiorski, K. Luszczyk, A. Baszczuk, Morphology and absorption properties control of silver nanoparticles deposited on two types of sol-gel sphercal silica substrates, J. Alloys Compd. 588 (2014) 70–74.
[2] K. Kadziola, I. Piwonski, A. Kisielewska, D. Szczukocki, B. Krawczki, J. Sielski, The photoactivity of titanium dioxide coatings with silver nanoparticles prepared by sol-gel and reactive magneton sputtering methodes-comparative studies, Appl. Surf. Sci. 288 (2014) 503–512.
[3] T. Gao, B.P. Jelle, A. Gustavsen, Core-shell-typed Ag@SiO_2 nanoparticles as solar selective coating materials, J. Nanopart. Res. 15 (2013) 1–9.
[4] W.M. Ye, W.W. Zhao, H.Z. Li, Z. Jie, S.J. Guo, P. Shi, Theoretical study of the local surface plasmon resonance properties of silver nanosphere clusters, Plasmonics 8 (2013) 1351–1360.
[5] K.L. Kelly, E. Coronado, L.L. Zhao, G.C. Schatz, The optical properties of metal nanoparticles: the influence of size, shape, and dielectric environment, J. Phys. Chem. B 107 (2003) 668–677.
[6] U. Kreibig, L. Genzel, Optical absorption of small metallic particles, Surf. Sci. 156 (1985) 678–700.
[7] H.C. Barshilia, P. Kumar, K.S. Rajam, A. Biswas, Structure and optical properties of Ag-Al_2O_3 nanocermet solar selective coatings prepared using unbalance dmagnetron sputtering, Sol. Energy Mater. Sol. Cells 95 (2011) 1707–1715.
[8] S. Sen, S. Mahanty, S. Roy, O. Heintz, S. Bourgeois, D. Chaumont, Investigation on sol-gel synthesized Ag-doped TiO_2 cermet thin films, Thin Solid Films 474 (2005) 245–249.
[9] H.C. Barshilia, A. Tanwer, J. Siju, D.B. Mahadik, A.V. Rao, Design of Ag-Si_3N_4 nanocermet coatings for photothermal conversion applications, Nanosci. Nanotechnol. Lett. 4 (2012) 41–47.
[10] S.K. Mandal, R.K. Roy, A.K. Pal, Effect of particle shape distribution on the surface plasmon resonance of Ag-SiO_2 nanocomposite thin films, J. Phys. D: Appl. Phys. 36 (2003) 261–265.
[11] P. Zhou, Y.Y. Hai, H.J. Jian, J. Li, T. Han, Y.W. Song, J.Z. Rong, X.Z. Yu, Y.C. Liang, Concentration and size dependence of optical properties of Ag:Bi_2O_3 composite films by using the co-sputtering method, Thin Solid Films 455 (2004) 605–608.
[12] X.X. Xiao, G. Xu, B. Xiong, D. Chen, L. Miao, The film thickness dependent thermal stability of Ag-Al_2O_3 thin films as high-temperature solar selective absorbers, J. Nanopart. Res. 14 (2012) 746.

[13] K. Sugawara, Y. Minamide, M. Kawamura, Y. Abe, K. Sasaki, Agglomeration behaviour of Ag films suppressed by alloying with some elements, Vacuum 83 (2009) 610–613.
[14] R. Sachan, S. Yadavali, N. Shirato, H. Krishna, V. Ramos, G. Duscher, S.J. Pennycook, A.K. Gangopadhyay, H. Garcia, R. Kalyanaraman, Self-organized bimetallic Ag-Co nanoparticles with tunable localized surface plasmons showing high environmental stability and sensitivity, Nanotechnology 23 (2012) 275604.
[15] G. Yang, J.B. Sun, J. Zhou, Dielectric properties of aluminum silver alloy thin film in optical frequency range, J. Appl. Phys. 109 (2011) 123105.
[16] E. Misra, T.L. Alford, Effect of alloying and cladding on the failure of silver metallization under hightemperature and current stressing, Appl. Phys. Lett. 87 (2005) 172111.
[17] K. Sugawara, M. Kawamura, K. Abe, K. Sasaki, Comparison of the agglomeration behavior of Ag(Al) films and Ag(Au) films, Microelectron. Eng. 84 (2007) 2476–2480.
[18] J.H. Gao, C.J. Tu, L.Y. Liang, H.L. Zhang, F. Zhuge, L. Wu, H.T. Cao, K. Yu, Silver nanoparticles with armor layer embedded in the alumina matrix to form nanocermet thin films with sound thermal stability, ACS Appl. Mater. Interfaces 6 (2014) 11550–11557.
[19] A. Pan, Z.P. Yang, H.G. Zheng, F.X. Liu, Y.C. Zhu, X.B. Su, Z.J. Ding, Changeable position of SPR peak of Ag nanoparticles embedded in mesoporous SiO_2 glass by annealing treatment, Appl. Surf. Sci. 205 (2003) 323–328.
[20] G. De, M. Gusso, L. Tapfer, Annealing behavior of silver, copper, and silver-copper nanoclusters in a silica matrix synthesized by the sol-gel technique, J. Appl. Phys. 80 (1995) 6734–6739.
[21] O.A. Yeshchenko, I.M. Dmitruk, A.A. Alexeenko, A.V. Kotko, J. Verdal, A.O. Pinchuk, Size and temperature effects on the surface plasmon resonance in silver nanoparticles, Plasmonics 7 (2012) 685–694.
[22] Z.Y. Zhang, T.M. Nenoff, K. Leung, S.R. Ferreira, J.Y. Huang, D.T. Berry, P.P. Provencio, R. Stumpf, Room-temperature synthesis of Ag-Ni and Pd-Ni alloy nanoparticles, J. Phys. Chem. C 114 (2010) 14309–14318.
[23] A. Pal, S. Shah, S. Devi, Synthesis of Au-Ag alloy nanoparticles in aqueous polymer solution, Colloids Surf. A: Physicochem. Eng. Aspects 302 (2007) 51–57.
[24] A.J. McAlister, The Ag-Al (silver-aluminum) system, Bull. Alloy Phase Diag. 8 (1987) 526–533.
[25] N.Z. Zarkevich, D.D. Johnson, Predicted hcp Ag-Al metastable phase diagram, equilibrium ground states, and precipitate structure, Phys. Rev. B 67 (2003) 064104.
[26] S. Duhan, S. Devi, M. Srivastava, Characterization of nanocrystalline Ag/SiO_2 nanocomposites and synthesis by wet chemical method, Ind. J. Pure Appl. Phys. 48 (2010) 271–275.
[27] U. Kreibig, M. Vollmer, Theoretical consideration Optical Properties of Metal Cluster, vol. 25, Springer, New York, 1995, pp. 13–201.
[28] A. Pinchuk, U. Kreibig, Interface decay channel of particle surface Plasmon resonance, New J. Phys. 5 (2003) 151.
[29] S. Berciaud, L. Cognet, P. Tamarat, B. Lounis, Observation of intrinsic size effects in the optical response of individual gold nanoparticles, Nano Lett. 5 (2005) 515–518.
[30] S.R. Bhattacharyya, D. Datta, I. Shyjumon, B.M. Smirnov, T.K. Chini, D. Ghose, R. Hippler, Growth and melting of silicon supported silver nanocluster films, J. Phys. D: Appl. Phys. 42 (2009) 035306.
[31] O.A. Yeshchenko, I.M. Dmitruk, A.A. Alexeenko, A.V. Kotko, Surface plasmon as a probe for melting of silver nanoparticles, Nanotechnology 21 (2010) 045203.
[32] R.C. Adochite, D. Munteanu, M. Torrell, L. Cunha, E. Alves, N.P. Barradas, A. Cavaleiro, J.P. Riviere, E.L. Bourhis, D. Eyidi, F. Vaz, The influence of annealing treatments on the properties of $Ag:TiO_2$ nanocomposite films prepared by magnetron sputtering, Appl. Surf. Sci. 258 (2012) 4028–4034.
[33] B. Vincent Crist, Handbook of Monochromatic XPS Spectra, The Elements and Native Oxides, Wiley, New York, 1999.
[34] G. De, G. Mattei, P. Mazzoldi, C. Sada, G. Battaglin, A. Quaranta, Au-Cu alloy nanocluster doped SiO_2 film by sol-gel processing, Chem. Mater. 12 (2000) 2157–2160.
[35] F. Tao, M.E. Grass, Y.W. Zhang, D.R. Butcher, J.R. Renzas, Z. Liu, J.Y. Chung, B.S. Mun, M. Salmeron, G.A. Somorjai, Reaction-driven restructuring of Rh-Pd and Pt-Pd core-shell nanoparticles, Science 322 (2008) 932–934.